

Article

Investigation of the Impact of Geotextile Incorporation on the Mechanical Properties of Geopolymer

Wei Zhou ¹, Xiujie Zhang ^{2,3}, Hongzhong Li ², Rongtao Yan ⁴, Xianlun Huang ⁵, Jianjun Gan ⁶ , Jinping Zhang ³, Xiaoyong Cheng ³, Junhong Yuan ⁷ and Bingxiang Yuan ^{5,*} 

¹ Gongdong Traffic Industrial Investment Company, Guangzhou 510101, China; fengye82922@126.com

² School of Civil Engineering, Guangdong Communication Polytechnic, Guangzhou 510650, China; zhangxiujie@ghdi.cn (X.Z.); lih2001@gdcp.edu.cn (H.L.)

³ Guangdong Province Communications Planning & Design Institute Group Co., Ltd., Guangzhou 510507, China; zhangjinpings@ghdi.cn (J.Z.); chengxiaoyong@ghdi.cn (X.C.)

⁴ School of Civil Engineering, Guilin University of Technology, Guilin 541000, China; 2012019@glut.edu.cn

⁵ School of Civil and Transportation Engineering, Guangdong University of Technology, Guangzhou 510006, China; 2112309008@mail2.gdut.edu.cn

⁶ Jiangxi Engineering Research Center of Water Engineering Safety and Resources Efficient Utilization, Nanchang Institute of Technology, Nanchang 330099, China; ganjianjun@nit.edu.cn

⁷ School of Civil Engineering, Inner Mongolia University, Hohhot 010070, China; yjh@imu.edu.cn

* Correspondence: yuanbx@gdut.edu.cn

Abstract: Geopolymers assume an irreplaceable position in the engineering field on account of their numerous merits, such as durability and high temperature resistance. Nevertheless, geopolymers also demonstrate brittleness. In this study, geotextiles with different layers were added to geopolymer to study its compressive strength and stability. Laboratory materials such as alkali activators, geotextiles and granite residual soil (GRS) were utilized. The samples were characterized via XRD, TG-DTG, SEM-EDS and FT-IR. The results indicate that the toughness of geopolymer is significantly enhanced by adding geotextiles, and the strength increase is most obvious when adding one layer of geotextile: the strength increased from 2.57 Mpa to 3.26 Mpa on the 14th day, an increase of 27%. Additionally, the D-W cycle has a great influence on geotextile polymers. On the 14th day, the average strength of the D-W cyclic sample (1.935 Mpa) was 1.305 Mpa smaller than that of the naturally cured sample (3.24 Mpa), and the strength decreased by 40%. These discoveries offer a novel approach for further promoting the application of geopolymers, especially in the field of foundation reinforcement.

Keywords: geotextile; granite residual soil; geopolymers; unconfined compression test; microanalysis



Citation: Zhou, W.; Zhang, X.; Li, H.; Yan, R.; Huang, X.; Gan, J.; Zhang, J.; Cheng, X.; Yuan, J.; Yuan, B.

Investigation of the Impact of Geotextile Incorporation on the Mechanical Properties of Geopolymer. *Buildings* **2024**, *14*, 2595. <https://doi.org/10.3390/buildings14092595>

Academic Editor: Mizan Ahmed

Received: 20 July 2024

Revised: 16 August 2024

Accepted: 21 August 2024

Published: 23 August 2024



Copyright: © 2024 by the authors. Licensee MDPI, Basel, Switzerland. This article is an open access article distributed under the terms and conditions of the Creative Commons Attribution (CC BY) license (<https://creativecommons.org/licenses/by/4.0/>).

1. Introduction

With the swift economic growth China has experienced in recent years, the prevalence of underground infrastructure like parking garages, shopping centers, and subway tunnels has surged [1,2]. However, the development of underground engineering generates substantial volumes of excavated soil, which is often disposed of through landfilling. This has led to numerous engineering mishaps due to inadequate waste management practices. For instance, the 2015 landslide at the Hongao waste disposal site in Guangming New District, Shenzhen, resulted in numerous fatalities, and the recent indiscriminate disposal of construction waste in Shanghai, where it was intermingled with household waste, led to significantly elevated levels of ammonia nitrogen [3,4]. Granite residual soil (GRS) is mainly distributed in the Minyue area of China, and it easily collapses when encountering water in engineering [5]. Over the past century, numerous scholars have investigated GRS and discovered that its alkali activation can produce geopolymers. Geopolymer is a kind of inorganic high polymeric gelled material which is usually composed of three-dimensional network gels polymerized by silica tetrahedron and aluminum oxide tetrahedron prepared by natural minerals or construction waste or aluminum silicate minerals formed by other

effects [6]. It has the excellent characteristics of good stability, good durability, high strength, permeability, and high temperature resistance.

In the field of the preparation of geopolymers, Perumal et al. [7] used alkali activation on geopolymers prepared from tailings from three different regions and found that the strength was only 7 MPa in 7 days. Temuujin et al. [8] used fly ash to prepare geopolymers, and the alkali intensification strength reached 9.2 MPa after calcination at a high temperature. Compared with other waste soil materials, GRS is rich in clay minerals, among which, kaolinite and alloxite account for more, and the Si and Al content is higher. The amount of seepage of Si and Al directly affects the formation of geopolymers [9], meaning that the compressive strength of geopolymers prepared after calcination reaches 50 MPa [10]. So, GRS has a good application prospect in new materials. Therefore, GRS is not only a common residue in southern China, but also has a high geopolymer strength. Hayder et al. [11] found that adding fly ash to kaolin can increase the strength of the material, but in this study, the influence of geotextiles on GRS polymers is discussed. In summary, GRS is the preferred material.

In recent years, GRS has been studied as a new material to replace ordinary Portland cement, and it has been applied to the reinforcement of weak foundations [12]. For example, a new type of cementitious material can be synthesized by using the alkali activation method to prepare geopolymers in combination with southern GRS. Zhang et al. [13] studied waste soil excavated with soil, which was thermally activated, and then, alkali excitation was used to prepare new cementitious material. It has good hydrocoagulability, and its strength can reach 65.63 MPa. When reviewing a study of the metakaolin preparation of geopolymers, it was also clearly emphasized that the low carbon footprint and superior properties of geopolymers render them a viable alternative to traditional Portland cement [8]. In the future development of low-carbon requirements, the use of traditional Portland cement will likely be phased out, thus positioning geopolymer materials as a promising avenue for advancement [10].

Zhang et al. found that the heat treatment of kaolin is usually required to obtain more reactive precursors, and thus, high-strength geopolymers [14]. Some scholars calcined kaolin for 2 h at 600 °C, 700 °C, and 800 °C and selected one of the samples as the precursor of geopolymer synthesis [11,15]. The results showed that calcination temperature plays an important role in the polymerization of geopolymers. A solution of 10 mol/L NaOH leads to the highest dissolution rate of Si^{4+} and Al^{3+} and the highest degree of polymerization of geopolymers [12,16].

However, considerable challenges are often revealed in real-world applications. For instance, geopolymers exhibit brittleness when utilized in foundation reinforcement, which will reduce their durability [13,14,17,18]. This brittleness can be attributed to the disordered nature of the geopolymer structure and the instability of the inorganic polymer composition, especially in humid environments where microbial growth degrades the material [15,19]. In order to solve these problems, we investigated the development of a new material that combines the advantages of geotextiles with the excellent properties of geopolymers.

In the field of civil materials, it is common to incorporate different fiber products into cement to significantly improve the physical, mechanical, and durability properties of cement fiber products [20]. Many studies have shown that adding fiber to geopolymers can improve the properties of geopolymers [21–23]. Noushini [24] conducted a comprehensive experimental study on the structure and material properties of synthetic fiber-reinforced geopolymers, proving the toughening effect of geotextile synthetic fibers on geopolymers. Korniejenko [25] studied the mechanical properties of fiber-reinforced geopolymers. The results showed that the addition of synthetic fiber improved the mechanical properties of the material. When the content of synthetic fiber was 0.5%, the compressive strength was the best, which increased by 167% compared with the reference sample without fiber. When the content of synthetic fiber was 0.75%, the flexural strength of the sample was the best and increased by 100%. Nematolla-hi [26] studied the influence of fibers with different volume fractions on the tensile, bending, and compression properties of geopolymer materials and

found that the optimal content was 1%, and the compressive strength would be reduced when the optimal content was exceeded. A geotextile is a common geomaterial, in which the addition of geotextile synthetic fiber can improve the tensile and bending strength, toughness, and impact resistance of a material through bridging cracks [23]. In addition, geotextile synthetic fiber can maintain the drying and stability of soil structure through its good water permeability and filtration. A geotextile is also a kind of fiber material, while non-woven geotextile is often used for reinforced soil [25]. Gas composition can promote material synthesis [27]. Due to its good permeability and relatively chaotic fiber structure, it can be preferentially used for reinforcing polymer materials, especially polyester filament geotextiles. At the same time, different layers of geotextiles also have a great impact on the reinforcement of soil [28].

Therefore, combined with the pulling force of geotextile fiber, a geotextile-reinforced geopolymer sample was prepared to compensate for the brittle damage prevalent in geotextiles. In order to study the enhancement effect of polymers with geotextiles, experiments were conducted to investigate their performance and to evaluate their performance within 14 days, and the effects of different layers of geotextiles on the properties were studied. Utilizing advanced laboratory techniques such as XRD, TG-DTG, SEM-EDS, and FT-IR, the properties of geotextile-reinforced geopolymers have been investigated. The findings indicate that geotextile incorporation substantially improves the toughness of geopolymers, providing new insights into the structure and interaction mechanisms of these materials. This innovative approach offers a potential solution for improving the durability of geopolymers and advancing materials science.

2. Materials and Methods

2.1. Materials

2.1.1. Granite Residual Soil

The GRS was collected about 5 m from a foundation pit in Huolushan, Guangdong Province, China. GRS is mostly mixed soil weathered by medium–fine granite, and the particle size is mainly distributed below 1.18 mm. In order to better simulate the actual foundation reinforcement situation, the experiment adopted GRS with a particle size of less than 1.18 mm. Accordingly, the strength of the geopolymer prepared with a 0.075 mm particle size was significantly reduced. The GRS was mechanically activated (particle size less than 1.18 mm) and activated at a high temperature (calcined at 650 °C). It can be seen from Figure 1b that there were various mineral components in the original soil. The GRS had high metakaolin content. XRD analysis was carried out on the original soil, as shown in Figure 2, which contained kaolinite, illite, microcline and quartz, with higher kaolinite content. The collected GRS was put into an oven with a temperature of 105 °C for 24 h to dry, and then ground by a ball mill to through a screen with an aperture of 1.18 mm. The soil with particle sizes of less than 1.18 mm was put into a muffle furnace for calcination, the calcination temperature was set at 650 °C for continuous calcination for 2 h, and the heating rate was 10 °C/min. After calcination, the soil temperature was reduced to room temperature and then sealed with a plastic bag and stored at room temperature for use. The apparent characteristics of the screened soil after calcination at 650 °C were bright yellowish-brown, as shown in Figure 1c.

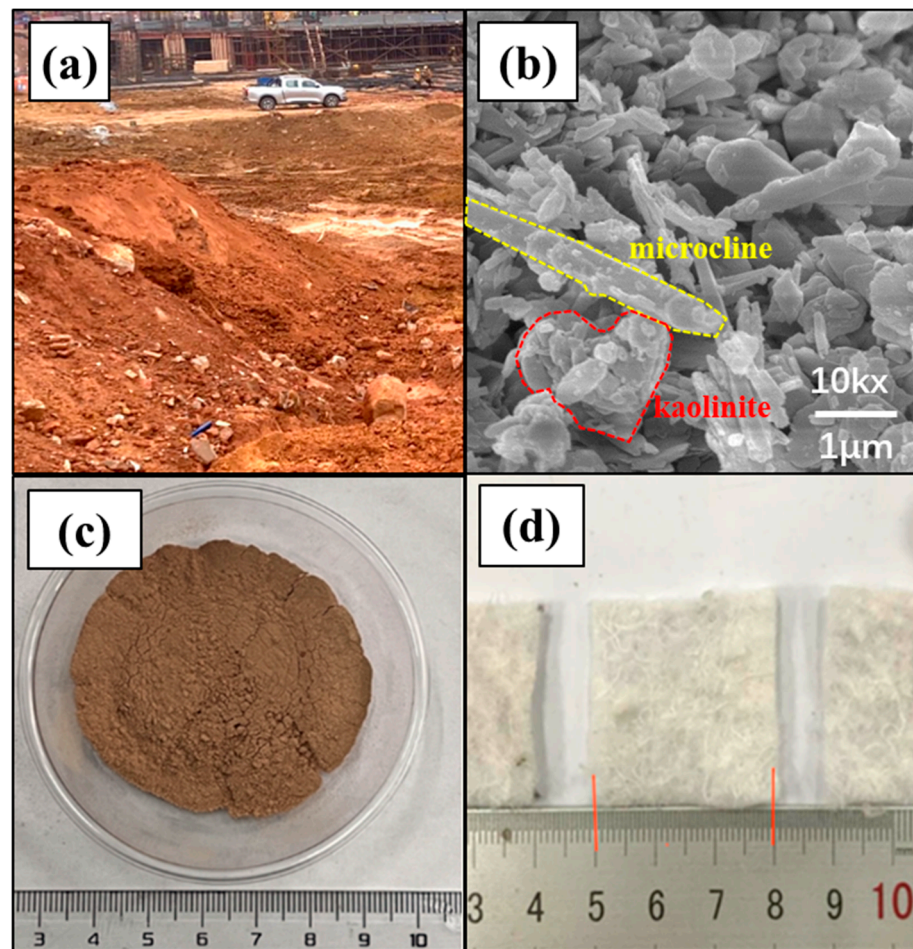


Figure 1. Picture of (a) soil sampling location, (b) SEM of original soil, (c) soil samples after calcination at 650 °C, (d) non-woven geotextile.

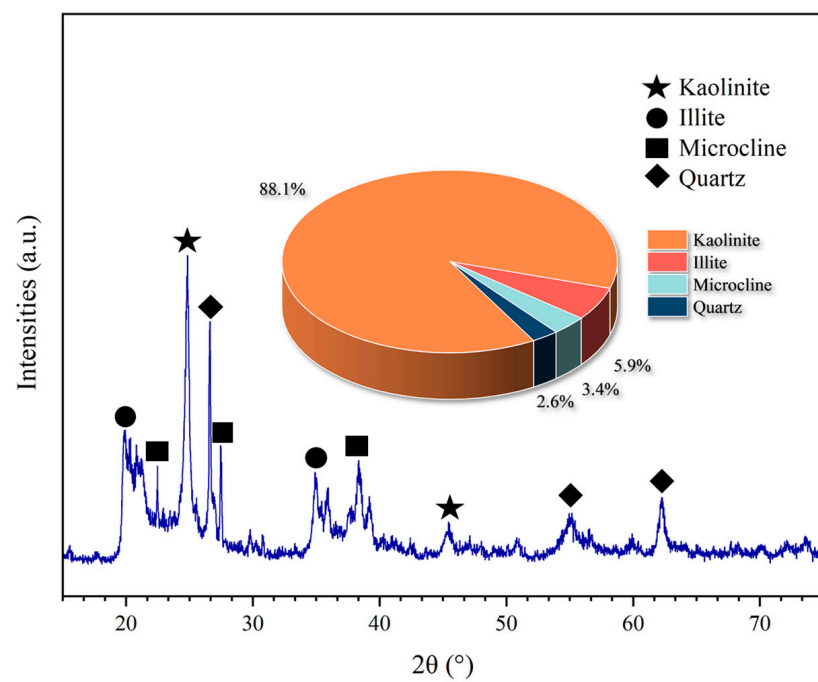


Figure 2. XRD patterns of GRS.

2.1.2. Geotextiles

The present study used non-woven PET 10–4.5–200 geotextiles, which were polyester filament geotextiles (Figure 1d). The geotextiles needed to not be cut too large, so as not to destroy the continuity of the geopolymer itself, which would have resulted in a significant reduction in the compressive strength of the geopolymer. The geotextile used in the test was 30 mm long and 30 mm wide, and the mass of each geotextile was about 0.07 g. Table 1 provides the properties of the tested geotextile.

Table 1. Properties of the tested geotextile.

Properties	Value	Test Method
Characteristic initial strength (kN/m)	10	ISO 10319 [29]
Nominal mass (g/m ²)	200	ISO 9864 [30]

2.1.3. Alkaline Solution

The alkaline solution was prepared from NaOH solution with a concentration of 10 mol/L and Na₂SiO₃ with a modulus of 3.33 according to the mass ratio of 2:1 (the ratio of silicon to sodium: 2:1).

2.2. Test Scheme

Using the above alkali solution, we prepared the polypropylene geotextile according to a liquid-to-solid ratio of 0.5. According to the number of layers of geotextile added and the curing conditions in the experiment, the samples were divided into 12 groups, marked as N-1 to C-3 (Table 2). Keeping the geotextile material constant, the reinforcing effect of the geotextile on the geotextile material was analyzed by changing the number of layers of geotextile and curing conditions.

Table 2. Experimental scheme of dry and wet cycle.

Sample	Number of Geotextile Layers	Curing Condition	Experiment Period/d	
N-0	0	Natural curing	7	14
N-1	1			
N-2	2			
N-3	3			
S-0	0	Soaking curing	7	14
S-1	1			
S-2	2			
S-3	3			
C-0	0	D-W cycle curing	7	14
C-1	1			
C-2	2			
C-3	3			

Preparation was carried out according to the proportions mentioned in Table 2. A cylindrical three-valve mold with a diameter of 39.1 mm and a height of 80.0 mm was selected as the sample mold. After the bubbles were discharged by stratified vibration, the mold was released for 24 h after curing at 25 °C.

The natural curing method used in this test was closed-box curing at 25 °C temperature and 60% humidity. The soaking curing of this test was carried out in a water curing box at 25 °C. The wet–dry cycle (D-W cycle) operation of this test was drying in an oven with a set temperature of 50 °C for 12 h as a “dry cycle”; the sample was placed in water curing at room temperature for 12 h as a “wet cycle”; this took place 24 h a day, with a “dry cycle” and a “wet cycle” constituting a “cycle”.

According to the Chinese standard ISO 679:2009 [31] “Cement strength test method—Strength determination”, the compressive strength test was carried out on the sample after

curing for 7 and 14 days. After strength testing, sample fragments were collected and immersed in absolute ethanol to partition the reaction for retention. Subsequent XRD, SEM, and TG testing and analysis took place.

The specific experimental steps are shown in Figure 3.



Figure 3. Sample preparation process.

2.3. Methods

2.3.1. Compressive Strength Test

The sample was put into a pressure testing machine for compression. The specific steps and requirements of the test refer to the test standard of ASTM D2166-00 [32]. The loading rate of the constant-pressure testing machine was 0.5 mm/min.

2.3.2. XRD Spectrum

An X-ray diffractometer was used for phase identification and analysis of the hydration products of ground polymer powder under different curing times. The scanning range of the diffractometer was set between 10° and 90°, with a copper target for the measurements.

2.3.3. Thermogravimetric Analysis

The hydration product samples of the terpolymers were analyzed using the Germany Netz's TG 209 F1 Libra vacuum-sealed high-precision thermogravimetric analyzer (TGA) in Shiyanjia Lab. In the temperature range of 10–800 °C, N₂ was used as a protective gas at a heating rate of 10 °C min.

2.3.4. Scanning Electron Microscope

The microstructure of hydrated products reinforced with geotextiles was studied using an Hitachi SU8010 (Hitachi, Tokyo, Japan) field emission scanning electron microscope (FE-SEM) in Shiyanjia Lab. A 15 nm Au-Pd coating was applied before testing to improve electrical conductivity and image quality.

2.3.5. Mass Loss

For samples with W-D cycles, after each cycle, the sample was removed from the oven, cooled to room temperature, and weighed using an electronic scale with an accuracy of ±0.01 g prior to being re-immersed in the water. Mass loss was the percentage of mass lost from each cycle to the first cycle drying.

2.4. Experimental Scheme

The geotextile reinforcement test group was set to 12 groups. Each group is named in the format 'M-No.', where 'M' stands for the curing method (natural curing, soaking curing, or D-W cycle curing) and 'No.' stands for the number of geotextile layers (0, 1, 2,

or 3). The distribution diagram of the number of geotextile layers is shown in Figure 4. Among them, each group of samples was divided into 7-day curing and 14-day curing. The specific experimental scheme is shown in Table 2.

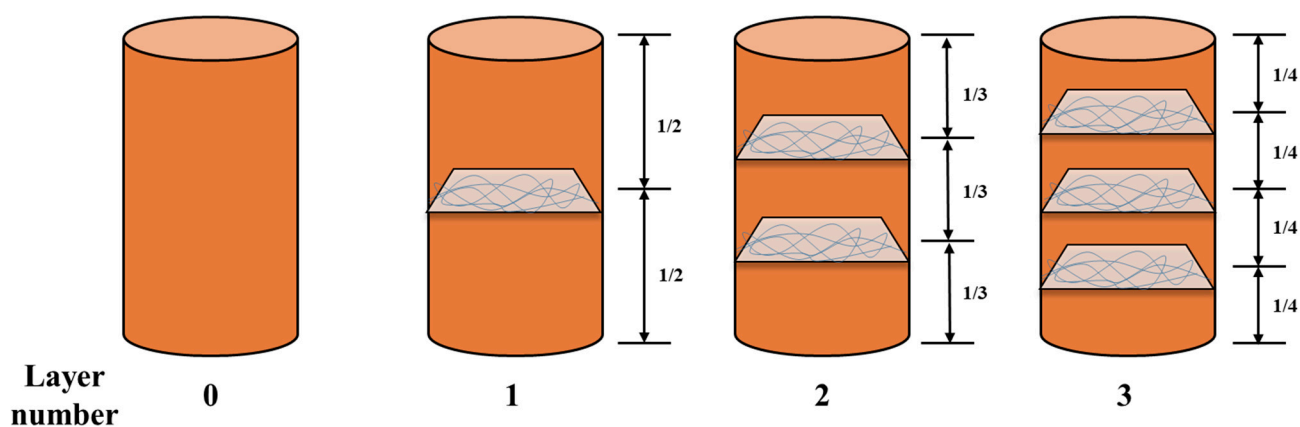


Figure 4. Arrangement of geotextile layers with different numbers of layers.

3. Results and Discussion

3.1. Compressive Strength

3.1.1. Influence of Geotextile Layers on Compressive Strength

The experimental results are shown in Figure 5. By comparing the 14-day compressive strength of specimens measured in groups N-0, N-1, N-2, and N-3 with the 14-day compressive strength measured in other groups, S-0 to S-3 and C-0 to C-3, it is evident that the compressive strength of groups N-1, N-2, and N-3 was significantly higher than that of group N-0 under the same curing conditions and curing time. Combined with other maintenance conditions, it can be seen that the reinforcement effect of the geotextile was brought by the geotextile itself. At the same time, it can be seen that the compressive strength measured with geotextile inclusion was higher than that without adding geotextiles; that is, geotextiles have a certain effect on improving the compressive strength of geopolymer. For materials without geotextiles, the form of failure is mainly shear failure close to 45° , accompanied by a slight bulge, as shown in Figure 6a. However, for the samples with geotextile added, the geotextile had anti-shear properties, which limited the swelling in the middle of the sample. Huang et al. [33] also clearly pointed out that fiber can inhibit the development and uplift of cracks. The failure form is the splitting failure at the top of the sample, which significantly increases its strength and does not cause a sudden stress drop, as shown in Figure 6b. This shows that geotextiles can be well combined with polymers, similar to the reinforced concrete structure of “steel” and “concrete”; with the geotextile acting as “steel” and the polymer as “concrete,” they can be effectively combined to leverage their respective strengths in a collaborative effort, so as to achieve the effect of improving the bearing capacity of members. Geotextiles are combined with geopolymers and work together to reinforce the geopolymer [34]. Under high pressure, the embedding effect of its fibers is more obvious [35]. Furthermore, it is worth noting that under the same curing conditions and curing time, the compressive strength of the N-3, S-3, and C-3 groups is a little different from that of the N-2, S-2, and C-2 groups. It can be concluded that under the same curing time and curing conditions, when the number of geotextile layers is greater than or equal to two layers, the effect of the number of geotextile layers and the distribution mode on the compressive strength of the geopolymer is almost negligible. This is mainly due to the loose structure around the fibers which weakens the bond of the material [33]. In the experimental study on the mechanism of the geotextile reinforcement of soft soil foundations, when the vertical pressure is constant and the number of layers added to the geotextile is no less than two layers, the improvement effect on the interface friction is not significant [17,18,36,37]. This conclusion is consistent with the results of this experiment.

At the same time, small deviations in the direction of the geotextile during the sampling process have a significant impact on the reinforcement effect [19,38]. As shown in Figure 5a, the strength of N-1 is anomalous, possibly due to the shift of the geotextile.

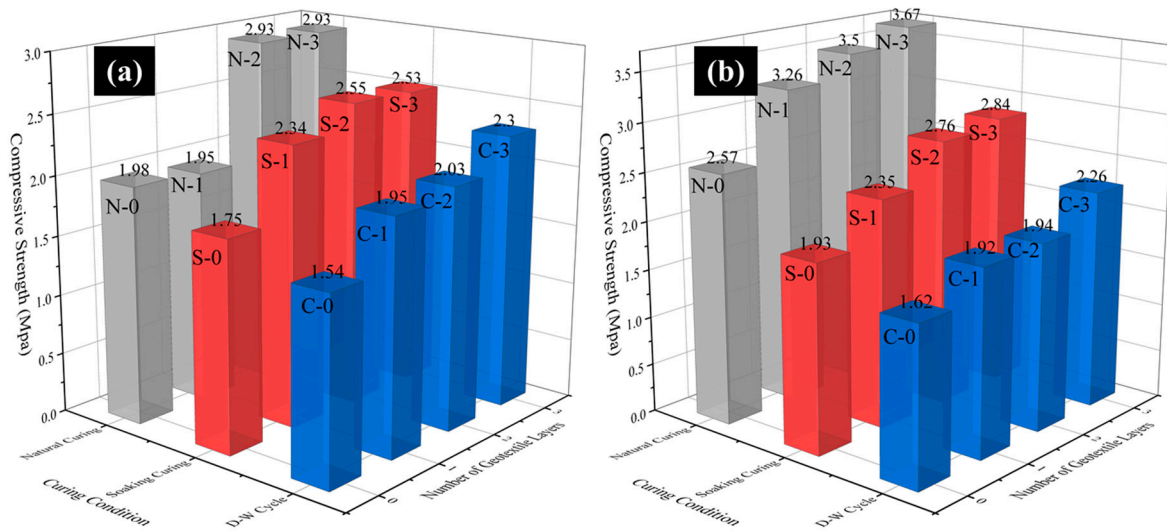


Figure 5. Effect of geotextile layer number and curing condition on compressive strength when curing for (a) 7 days and (b) 14 days.

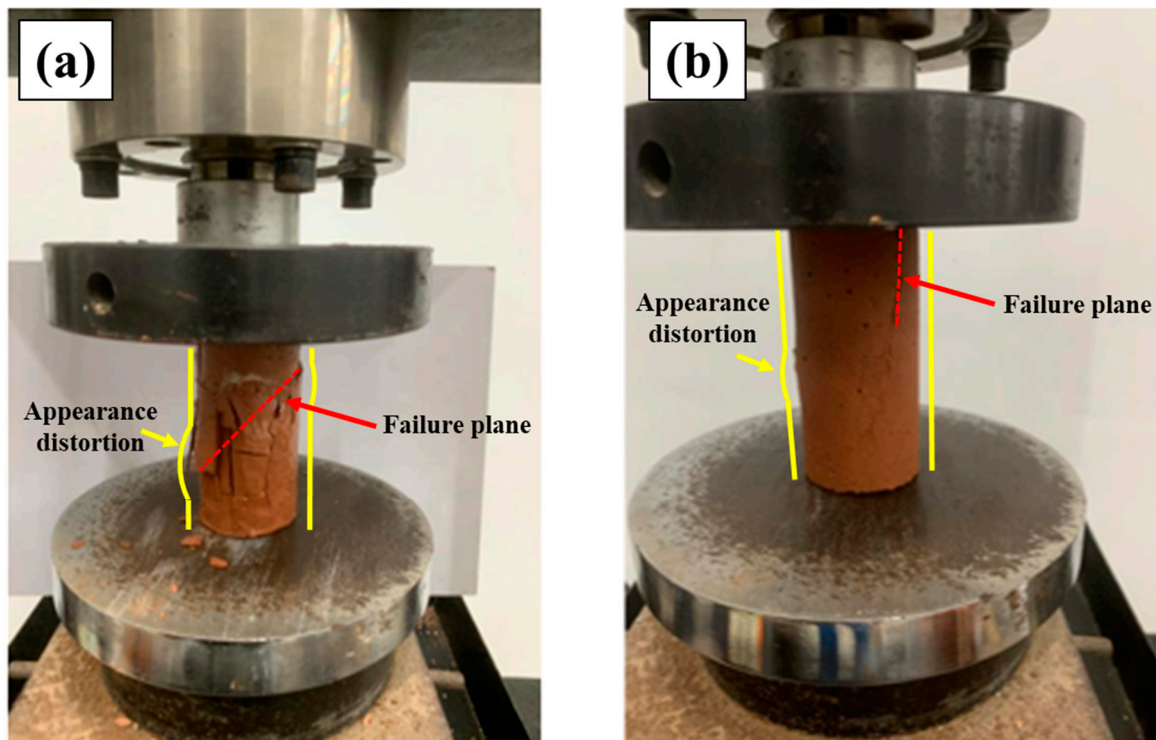


Figure 6. Failure state of unconfined compression test (a) sample without geotextile; (b) sample of a layer of geotextile.

3.1.2. Effect of Curing Conditions on Compressive Strength

As depicted in Figure 5, under the condition that the number of geotextile layers and the distribution mode are the same, the curing conditions and curing time have obvious influences on the compressive strength of geopolymers. The strength of the geopolymer was strongest under natural curing, followed by D-W cycle curing, and it was weakest

under water curing. In addition, under the same conditions regarding the number and distribution of geotextile layers, the curing time differentially impacts the compressive strength of geopolymers based on the curing method. Under natural curing conditions, the strength after 14 days was obviously higher than that after 7 days. Under the condition of D-W cycle curing, the strength after the curing time of 14 days was higher than that after the curing time of 7 days. Under the condition of soaking water curing, the strength after the curing time of 14 days decreased slightly compared with that after 7 days, but the decrease was not obvious. It is worth noting that in the D-C cycle, the strength of the samples without geotextiles increased from day 7 to day 14, but the strength of the samples with geotextiles decreased. It is obvious that soaking water maintenance has a certain negative impact on geotextiles. The effect is mainly due to the D-W cycle, which makes water continuously carry away the incomplete geopolymer precursor and then inhibits the geopolymer reaction. Moreover, Wu et al. also pointed out that soil particles containing water have a supporting effect on shear strength [20,39]. In this experiment, there may have been unreacted soil particles that experienced a decrease in strength due to water.

The air-entraining effect theory involves the incorporation of air-entraining agents within cementitious materials to stabilize microbubbles, which, upon the material's setting, form intricate porosities. This phenomenon substantially augments the durability of the cementitious materials [40]. During the fabrication of samples, the introduction of geotextiles into the geopolymer can adsorb these minuscule bubbles, potentially enhancing the material's endurance. When subjected to D-W cyclic curing, the samples exhibited a relatively minor decline in compressive strength due to the interplay between the beneficial air-entraining effect and the detrimental dilution of the alkaline solution concentration from water immersion. It is hypothesized that once the alkaline solution has fully reacted during the geopolymerization process, there will be a marked increase in the specimen's durability.

3.2. Hydration Mechanism of Geotextile-Enhanced Geopolymer

3.2.1. XRD Analysis

Figure 7a shows the XRD analysis results of GRS after calcination at 650 °C. Compared with the XRD results of the original soil, it can be seen that the characteristic diffraction of kaolinite at 12.26° disappeared, while the amorphous structure appeared at 30°~40°, indicating that kaolinite forms an amorphous structure at high temperatures during the process of heating and calcination [10]. Compared with the XRD of calcined soil at 650 °C (Figure 7a), the wave peaks of the geopolymers (Figure 7b) showed more peaks, which were mainly the polymers generated by the geopolymerization reaction. The mineral, which was mainly quartz stone, did not react, which is because quartz stone still has a high degree of stability at high temperatures.

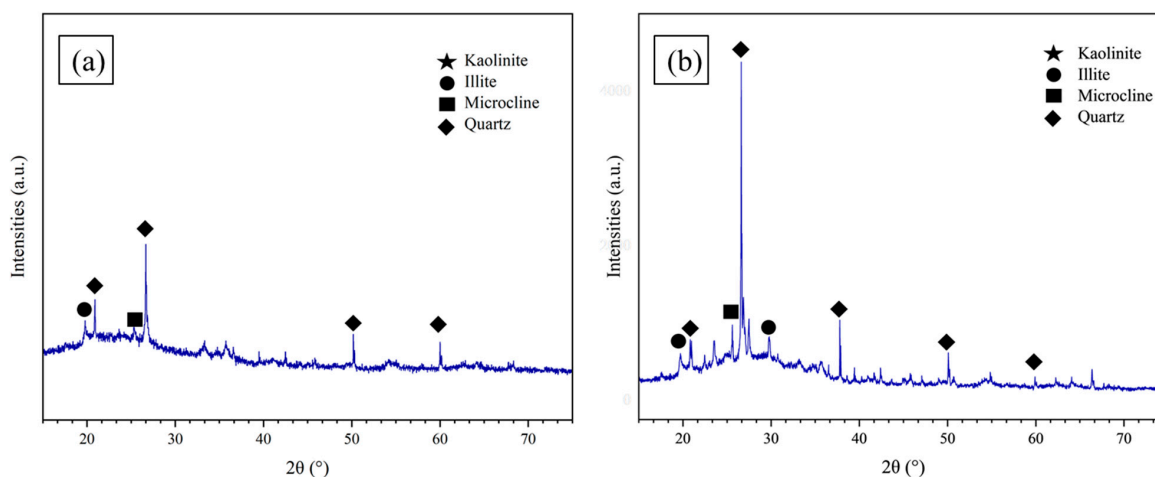


Figure 7. XRD of (a) calcined soil at 650 °C; (b) geopolymer.

3.2.2. TG-DTA

In order to study the thermal mass loss process of geopolymers prepared from GRS, a TG test was carried out, and the test results are shown in Figure 8.

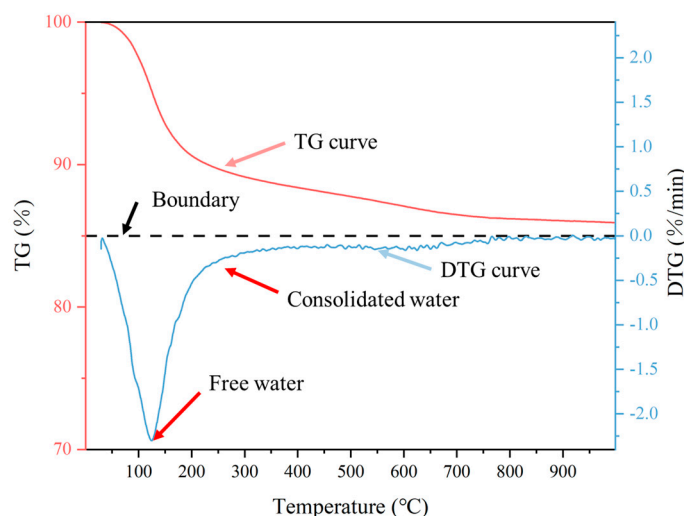


Figure 8. TG curve of geopolymer.

As can be seen from the TG curve in the figure, in the range of 30~200 °C, the residual mass decreased from 99.97% to 90.58%, which was due to the removal of free water adsorbed on clay minerals, resulting in a mass loss of 9.39% [21,41]. In the range of 200~400 °C, the mass loss was relatively small, because the interlayer water was removed, and the residual mass dropped to 88.40%; that is, the mass loss was 2.18%. When the temperature was 800 °C, the residual mass fraction of the TG curve decreased to 86.16%; that is, in the range of 400~800 °C, the residual mass decreased by 2.24%. When the calcination temperature reached 1000 °C, the residual mass fraction decreased to 85.93%, which indicated that the mass loss in the whole process of heating calcination was 14.04%. It can be seen that the geopolymer showed very strong thermal stability at high temperatures.

3.2.3. SEM Analysis

The samples reinforced with geotextiles were compressed and destroyed by unconfined compression experiments, and the geotextiles inside the samples, including some geotextiles bonded to the geotextiles, were taken out as experimental materials for scanning electron microscope analysis. The SEM imaging results of the sample from this study are presented in Figure 9. It can be seen that there were many traces of fiber pull in the damaged section. Through SEM images (Figure 10a), it can be clearly seen that the fibers provided pulling force inside the ground polymers. Despite the internal fiber net weaving being chaotic and disordered, most of the fibers were covered by geoprene, and there were many geoprene particles attached to the geoprene, resulting in grain accumulation, and the bonding between the geopolymers was relatively sufficient (Figure 11), which is conducive to the conduction of force. Thus, the tensile properties of geotextiles can be utilized in practical engineering applications. The compressive strength test results provide theoretical support for the use of geotextiles to improve the compressive strength of geopolymers.

Geotextiles themselves are often used as the “anti-filter layer” of drainage systems to meet the requirements of tunnel drainage by inhibiting the massive loss of soil particles caused by the permeability caused by water flow [25,26,42,43]. From the scanning electron microscope image with a magnification of 500 times (Figure 10b), it can be seen that multiple tiny pores formed due to the existence of the geotextiles, and no crystallization blockage was caused, leaving enough channels for the drainage of the geotextiles [27,44].

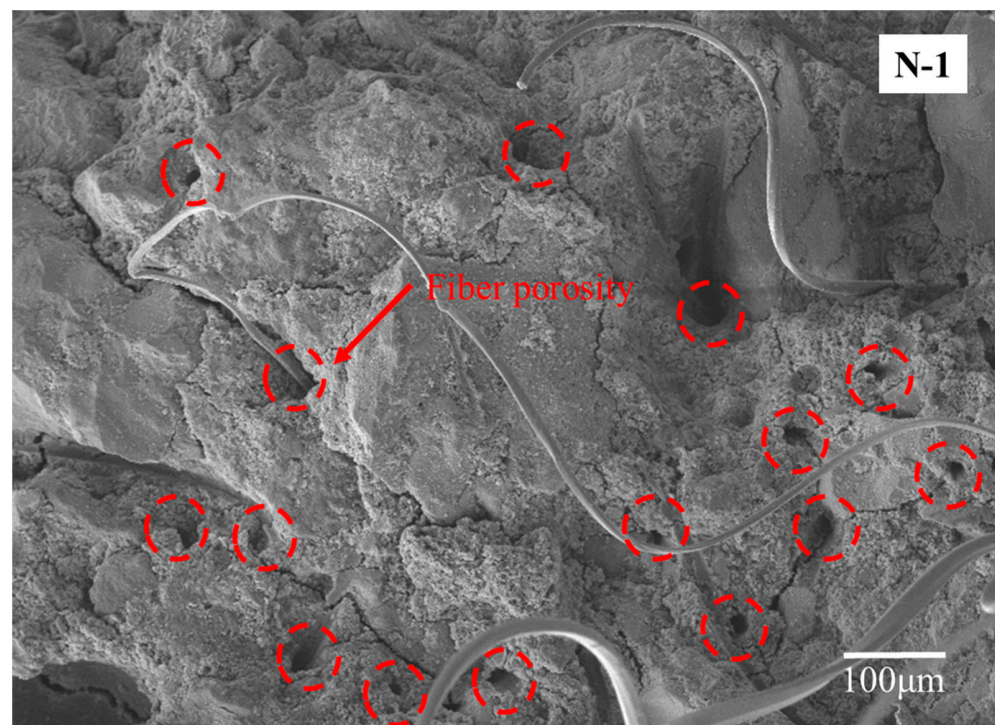


Figure 9. SEM of N-1 fracture surface.

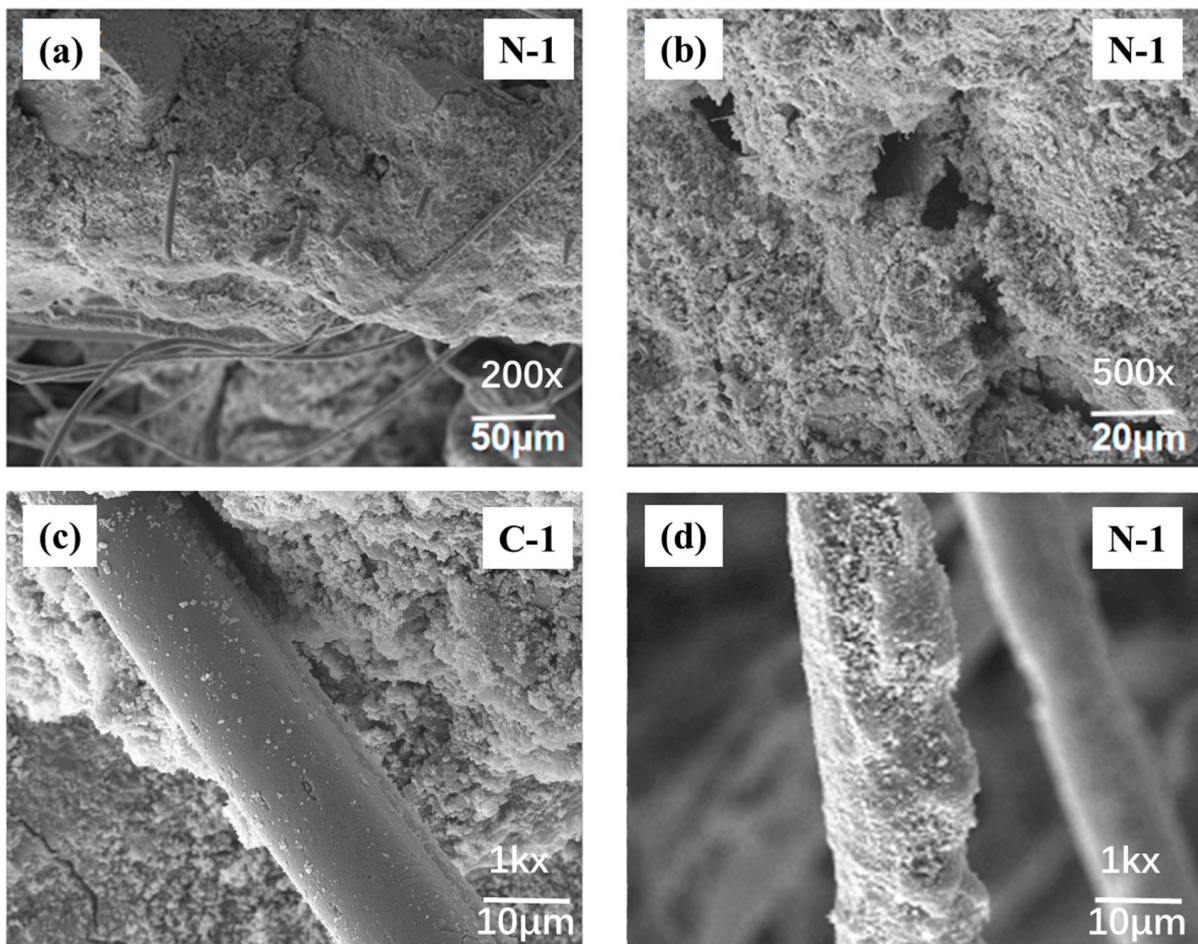


Figure 10. SEM of damaged samples: (a) 50 μm, (b) 20 μm, (c) 2 μm, (d) 1 μm.

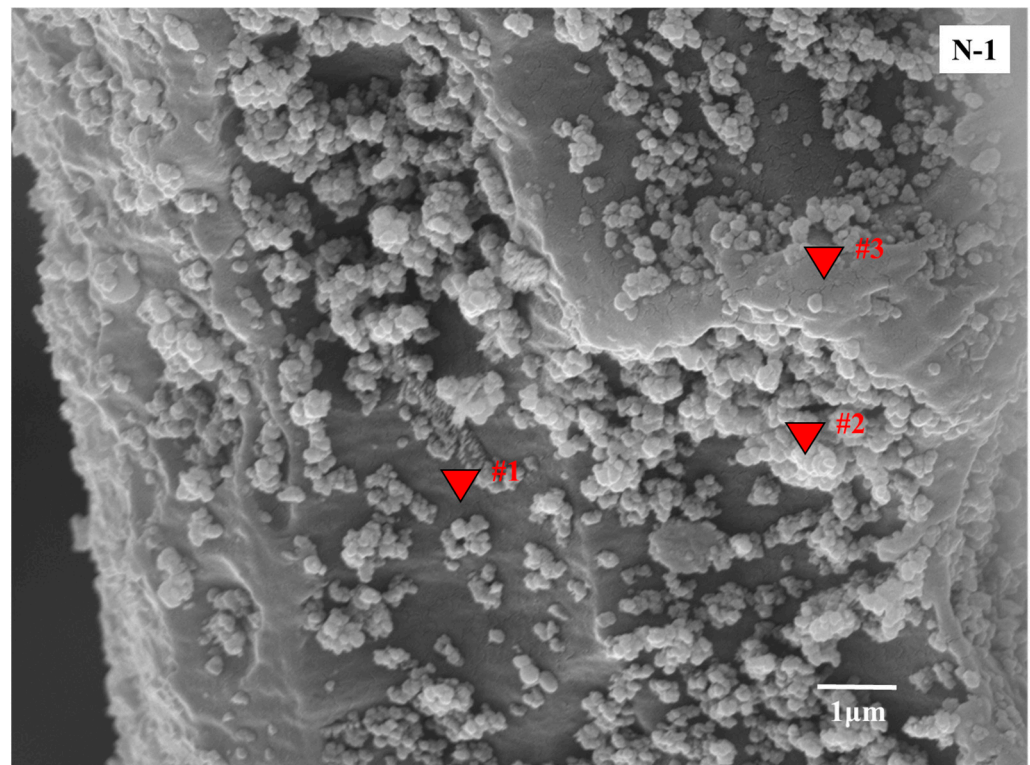


Figure 11. SEM of fibers on the polymers magnified by 10,000 times.

Obviously, the reduction in geopolymer strength with curing time may have been due to the presence of geotextiles forming more water channels. The polymer reaction of the GRS base was different from the cement reaction, and no hydration reaction occurred [12,16]. The silicon ion concentration of liquid in the sample affected the strength of the geopolymer, and the formation of the geopolymer was not promoted by water curing. Instead, the diluted concentration of silicon ions affected its strength [28,45]. Compared with Figure 10c,d, the fiber surface in C-1 was smoother than that of C-1, and there was less adhesion of the geopolymers. Therefore, under the condition of dry and wet cycle maintenance, because the free water infiltration specimen was repeatedly tested, the above dilution effect on aluminum and silicon ions was more significant, which greatly reduced the internal polymerization reaction, thus reducing its integrity [46,47].

3.2.4. EDS Analysis of Geotextile Geopolymer

According to the sample spectrum analysis in Figure 11, it can be seen that Al/Si values at #1, #2, and #3 were all 72–78%, and it can be seen that the chemical composition distribution inside the geopolymer was relatively uniform, and the proportions of Na and Si elements were smaller than those at #2 and #3 in the grain accumulation part due to the lack of grain accumulation in part #1. It can be inferred that the scanning electron microscope image here is the scanning image of the geopolymer attached to the geotextile fiber, the crystal accumulation part of the surface is the geopolymer, and the interior is the geotextile.

Based on the analysis of the elemental composition of the local polymer map, it can be determined that in addition to the main C and O elements, #1 and #3 contain a small amount of K element, including Na, Al, and Si elements, indicating that the main component here is kaolinite. The presence of K element was not detected in #2, while Al and Si elements were also present. The main composition of the surface here was alum inosilicate mineral, namely quartz. Quartz has the property of high temperature resistance. Under the high-temperature calcination of 650 °C, its internal structure did not change. Therefore, it still showed an obvious granular structure in #2. In #1 and #3, there were obvious plate or

layer structures, which were similar to those in the SEM images of kaolinite. From the EDS analysis and microscopic results (Table 3), it is easy to see that the geopolymer after the reaction could be more effectively bonded with the fibers of the geotextile to achieve the reinforcement effect.

Table 3. EDS analysis results.

#1		#2		#3	
Atom	Ratio/%	Atom	Ratio%	Atom	Ratio%
C	76.78	C	73.36	C	74.39
N	0.00	N	0.00	N	0.00
O	18.11	O	19.62	O	18.57
Na	2.05	Na	2.57	Na	2.57
Al	1.30	Al	1.93	Al	1.93
Si	1.68	Si	2.51	Si	2.65
K	0.08	K	0.00	K	0.05

3.3. Mass Loss Research

It can be observed from Figure 12 that the samples lost mass after each D-W cycle. It can be seen that the mass loss with two or three layers of geotextile polymer reached 3% during the tenth cycle. Under the same D-W cycle curing conditions, with the increase in the number of geotextile layers, the greater the increase in mass loss became. As shown in Figure 13, the D-W cycle significantly increased the development of cracks. From the perspective of the overall data, the quality of the samples had a downward trend during the D-W cycles, which was consistent with the disintegration of the samples themselves during the D-W cycles. The more reinforced layers of geotextile there were, the greater the proportion of the sample that fell off. Combined with the microstructure analysis, the addition of geotextile fibers led to the increase in the permeability of the sample. In the process of D-W cycles, the water of the sample was more volatile, which was accompanied by faster small-scale soil disintegration, but this situation is optimistic [30,48].

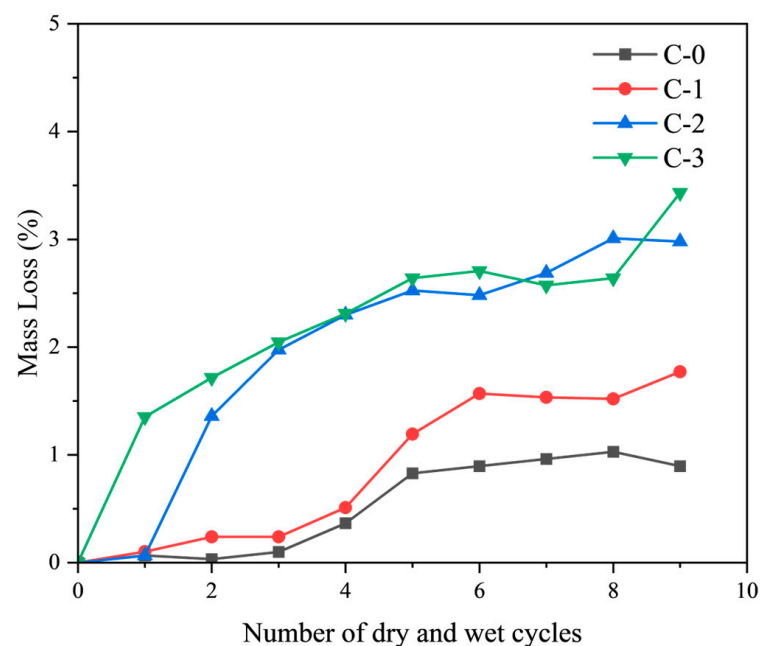


Figure 12. Mass loss of geopolymers with 0, 1, 2, and 3 geotextile layers (C-0, C-1, C-2, and C-3).



Figure 13. Cracks in D-W cycle samples.

The crack rate of soil is one of the most important macroscopic performance indexes under D-W cycles [31,49]. The crack rate reflects the degree of dry shrinkage cracking of soil under D-W cycles. The fractal dimension can characterize the disordered class of soil fracture growth under dry and wet cyclic action [32,50]. By observing the surface of a sample, it can be found that after several D-W cycles, cracks will appear on the surface, which will affect the mechanical properties such as the compressive strength of the geopolymer, and this influence is often unfavorable to the structural system in general.

Since the drying time, soaking time, and other conditions were the same, it can be considered that the possible water in the sample that had not completely dried was approximately the same; that is, it can be considered that the mass reduction in the sample was caused by the disintegration of the sample soil.

4. Conclusions

Geotextile-reinforced geopolymers, prepared using an alkali solution from GRS, were subjected to compression tests and microscopic analysis under varying curing durations and conditions. Based on the experimental outcomes, the following conclusions are drawn:

1. The geotextile has a strengthening effect on the geopolymer. Under the same curing time and conditions, the unconfined compressive strength of the samples with the geotextile was higher than that without the geotextile, and the compressive strength of the sample under 14-day natural curing increased from 2.57 Mpa to 3.26 Mpa, an increase of 27%.
2. The compressive strength of the geopolymer did not increase directly with the increase in the number of geotextile layers. With consistent curing time and conditions, the compressive strength of the geopolymer sample with a layer of geotextile cured for 14 days increased by 23% on average compared with the sample without geotextiles, while the subsequent increase in the number of geotextile layers resulted in a small increase in compressive strength, and the optimal average value only increased by 9%. Once the number of geotextile layers in the sample reached two or more layers, the impact on the geopolymer strength became negligible and gradually decreased.
3. The longer the curing time, the higher the polymer strength. But increasing the number of D-W cycle exacerbated the destruction of geopolymers. On the 14th day, the average strength of the D-W cyclic sample (1.935 Mpa) was 1.305 Mpa smaller than that of the naturally cured sample (3.24 Mpa), and the strength decreased by 40%. Under the condition of natural curing and soaking curing, the compressive strength of the geopolymer increased with the increase in time within 14 days.

However, the compressive strength of the geopolymer decreased slightly under the D-W cycle condition.

4. D-W cycles are unfavorable to geopolymers with geotextiles. With equal geotextile layer counts, distribution patterns, and curing times, the compressive strength of geopolymers cured naturally was markedly higher than those cured under D-W cycle conditions, which in turn were lower than those of geopolymers cured under the first two curing scenarios. But the strength of the geopolymer without geotextiles increased from day 7 to day 14. This was attributed to the effect of the geotextile on the concentration of alkali solution due to the enhanced penetration strength of the sample. This could be attributed to the wet–dry cycle which intensified the shedding of geopolymers.
5. Obviously, the layering of a whole geotextile added fine fibers to the sample to improve the compressive properties of the sample, which could effectively inhibit the development of cracks in the material. Geopolymers and geotextiles can strengthen a foundation together, which is of great significance for developing common technology involving geopolymer reinforcement and geotextile layering in foundation reinforcement. Both are environmentally friendly materials, which can reduce environmental pollution. Although the results show positive results regarding the geopolymerization and strength enhancement of residual soil reinforced by geotextiles, the results may be limited by the size of the laboratory, and it is suggested that to address the latter, we could appropriately increase the sample size to better simulate the field situation.

Author Contributions: Conceptualization, W.Z.; Methodology, X.Z.; Validation, H.L. and J.Z.; Project Administration, W.Z.; Investigation, X.Z.; Software, R.Y. and J.G.; Formal Analysis, R.Y. and B.Y.; Resources, H.L. and J.G.; Data Curation, J.Z.; Writing—Original Draft Preparation, X.H.; Writing—Review and Editing, X.H.; Visualization, X.C. and J.Y.; Supervision, X.C. and J.Y.; Funding Acquisition, B.Y. All authors have read and agreed to the published version of the manuscript.

Funding: This research was funded by the National Natural Science Foundation of China (No. 52278336), Guangdong Basic and Applied Research Foundation (No. 2023B1515020061 and 2022A1515240037), and Guangdong Key Scientific Research Platform and Project for General Universities (No. 2023CJPT003).

Data Availability Statement: Data are contained within the article.

Acknowledgments: The authors would gratefully like to acknowledge the support provided by the National Natural Science Foundation of China, Guangdong Basic and Applied Research Foundation, and Guangdong Key Scientific Research Platform and Project for General Universities. The help from Shiyanjia Lab (<http://www.shiyanjia.com>, accessed on 9 April 2024) in performing SEM experiments is greatly appreciated.

Conflicts of Interest: Author Wei Zhou was employed by the company Gongdong Traffic Industrial Investment Company. Authors Xiujie Zhang, Jinping Zhang and Xiaoyong Cheng were employed by the company Guangdong Province Communications Planning & Design Institute Group Co., Ltd. The remaining authors declare that the research was conducted in the absence of any commercial or financial relationships that could be construed as a potential conflict of interest.

References

1. Cui, C.; Liang, Z.; Xu, C.; Xin, Y.; Wang, B. Analytical Solution for Horizontal Vibration of End-Bearing Single Pile in Radially Heterogeneous Saturated Soil. *Appl. Math. Model.* **2023**, *116*, 65–83. [[CrossRef](#)]
2. Yuan, B.; Liang, J.; Lin, H.; Wang, W.; Xiao, Y. Experimental Study on Influencing Factors Associated with a New Tunnel Waterproofing for Improved Impermeability. *J. Test. Eval.* **2024**, *52*, 20230417. [[CrossRef](#)]
3. Meng, K.; Cui, C.; Liang, Z.; Li, H.; Pei, H. A New Approach for Longitudinal Vibration of a Large-Diameter Floating Pipe Pile in Visco-Elastic Soil Considering the Three-Dimensional Wave Effects. *Comput. Geotech.* **2020**, *128*, 103840. [[CrossRef](#)]
4. Yuan, B.; Sun, M.; Xiong, L.; Luo, Q.; Pradhan, S.P.; Li, H. Investigation of 3D Deformation of Transparent Soil around a Laterally Loaded Pile Based on a Hydraulic Gradient Model Test. *J. Build. Eng.* **2020**, *28*, 101024. [[CrossRef](#)]

5. Dou, H.; Wang, R.; Wang, H.; Jian, W. Rainfall Early Warning Threshold and Its Spatial Distribution of Rainfall-Induced Landslides in China. *Rock. Mech. Bull.* **2023**, *2*, 100056. [[CrossRef](#)]
6. Liew, Y.-M.; Heah, C.-Y.; Mohd Mustafa, A.B.; Kamarudin, H. Structure and properties of clay-based geopolymers: A review. *Prog. Mater. Sci.* **2016**, *83*, 595–629. [[CrossRef](#)]
7. Perumal, P.; Piekkari, K.; Sreenivasan, H.; Kinnunen, P.; Illikainen, M. One-Part Geopolymers from Mining Residues—Effect of Thermal Treatment on Three Different Tailings. *Miner. Eng.* **2019**, *144*, 106026. [[CrossRef](#)]
8. Temuujin, J.; van Riessen, A. Effect of Fly Ash Preliminary Calcination on the Properties of Geopolymer. *J. Hazard. Mater.* **2009**, *164*, 634–639. [[CrossRef](#)]
9. Cong, P.; Cheng, Y. Advances in Geopolymer Materials: A Comprehensive Review. *J. Traffic Transp. Eng.* **2021**, *8*, 283–314. [[CrossRef](#)]
10. Yuan, B.; Liang, J.; Li, X.; Zhang, B.; Luo, Q.; Sabri, S.M.M.; Muhammad, F.; Azzam, W.R.; Rao, F.; Yuan, P. Sustainable Utilization of Clay Minerals-Rich Engineering Muck via Alkali Activation: Optimization of Pore Structure by Thermal Treatment. *Appl. Clay Sci.* **2024**, *258*, 107491. [[CrossRef](#)]
11. Abdullah, H.H.; Shahin, M.A.; Sarker, P. Use of Fly-Ash Geopolymer Incorporating Ground Granulated Slag for Stabilisation of Kaolin Clay Cured at Ambient Temperature. *Geotech. Geol. Eng.* **2019**, *37*, 721–740. [[CrossRef](#)]
12. Hou, Z.; Liu, Y.; Han, Z.; Tang, M.; Gong, X.; Su, D.; Wang, L. Experimental Study of the Bearing Characteristics of a Novel Energy-Saving and Environmentally Friendly Pile: Drilling with Prestressed Concrete Pipe Cased Piles. *Int. J. Geomech.* **2024**, *24*, 04024035. [[CrossRef](#)]
13. Zhang, X.; Zhang, X.; Li, J.; Su, L.; Liu, J. Study of the Damage Mechanism on Mechanical Properties of Super Absorbent Polymer-Improved Geopolymers under Dry-Wet Cycling. *J. Mater. Sci.* **2024**, *59*, 4662–4679. [[CrossRef](#)]
14. Zhang, Z.H.; Zhu, H.J.; Zhou, C.H.; Wang, H. Geopolymer from kaolin in China: An overview. *Appl. Clay Sci.* **2016**, *119*, 31–41. [[CrossRef](#)]
15. Wang, H.; Li, H.; Wang, Y.; Yan, F. Preparation of Macroporous Ceramic from Metakaolinite-Based Geopolymer by Calcination. *Ceram. Int.* **2015**, *41*, 11177–11183. [[CrossRef](#)]
16. Yuan, B.; Liang, J.; Zhang, B.; Chen, W.; Huang, X.; Huang, Q.; Li, Y.; Yuan, P. Optimized reinforcement of granite residual soil using a cement and alkaline solution: A coupling effect. *J. Rock. Mech. Geotech. Eng.* **2024**. [[CrossRef](#)]
17. Yuan, B.; Chen, W.; Li, Z.; Zhao, J.; Luo, Q.; Chen, W.; Chen, T. Sustainability of the polymer SH reinforced recycled granite residual soil: Properties, physicochemical mechanism, and applications. *J. Soils Sediments* **2023**, *23*, 246–262. [[CrossRef](#)]
18. Yuan, B.; Li, Z.; Zhao, Z.; Ni, H.; Su, Z.; Li, Z. Experimental study of displacement field of layered soils surrounding laterally loaded pile based on transparent soil. *J. Soils Sediments* **2021**, *21*, 3072–3083. [[CrossRef](#)]
19. Yuan, B.; Chen, W.; Zhao, J.; Li, L.; Liu, F.; Guo, Y.; Zhang, B. Addition of alkaline solutions and fibers for the reinforcement of kaolinite-containing granite residual soil. *Appl. Clay Sci.* **2022**, *228*, 106644. [[CrossRef](#)]
20. Nassar, R.-U.-D.; Soroushian, P.; Balachandra, A.; Nassar, S.; Weerasiri, R.; Darsanasiri, N.; Abdol, N. Effect of Fiber Type and Content on the Performance of Extruded Wood Fiber Cement Products. *Case Stud. Constr. Mater.* **2022**, *16*, e00968. [[CrossRef](#)]
21. Farhan, N.A.; Sheikh, M.N.; Hadi, M.N.S. Behaviour of Ambient Cured Steel Fibre Reinforced Geopolymer Concrete Columns Under Axial and Flexural Loads. *Structures* **2018**, *15*, 184–195. [[CrossRef](#)]
22. Farhan, N.A.; Sheikh, M.N.; Hadi, M.N.S. Experimental Investigation on the Effect of Corrosion on the Bond Between Reinforcing Steel Bars and Fibre Reinforced Geopolymer Concrete. *Structures* **2018**, *14*, 251–261. [[CrossRef](#)]
23. Shaikh, F.U.A.; Fairchild, A.; Zammam, R. Comparative Strain and Deflection Hardening Behaviour of Polyethylene Fibre Reinforced Ambient Air and Heat Cured Geopolymer Composites. *Constr. Build. Mater.* **2018**, *163*, 890–900. [[CrossRef](#)]
24. Noushini, A.; Hastings, M.; Castel, A.; Aslani, F. Mechanical and Flexural Performance of Synthetic Fibre Reinforced Geopolymer Concrete. *Constr. Build. Mater.* **2018**, *186*, 454–475. [[CrossRef](#)]
25. Korniejenko, K.; Lin, W.-T.; Simonova, H. Mechanical Properties of Short Polymer Fiber-Reinforced Geopolymer Composites. *J. Compos. Sci.* **2020**, *4*, 128. [[CrossRef](#)]
26. Nematollahi, B.; Qiu, J.; Yang, E.-H.; Sanjayan, J. Micromechanics Constitutive Modelling and Optimization of Strain Hardening Geopolymer Composite. *Ceram. Int.* **2017**, *43*, 5999–6007. [[CrossRef](#)]
27. Zhang, H.; Bian, H.; Qi, S.; Wang, J. A Comprehensive Analysis of Formation Conditions, Intrinsic Properties, and Mechanical Responses of Gas Hydrate-Bearing Sediments. *Rock. Mech. Bull.* **2024**, *3*, 100114. [[CrossRef](#)]
28. Jayawardane, V.S.; Anggraini, V.; Li-Shen, A.T.; Paul, S.C.; Nimbalkar, S. Strength Enhancement of Geotextile-Reinforced Fly-Ash-Based Geopolymer Stabilized Residual Soil. *Int. J. Geosynth. Ground Eng.* **2020**, *6*, 50. [[CrossRef](#)]
29. ISO 679:2009; Cement—Test Methods—Determination of Strength. ISO: Geneva, Switzerland, 2009.
30. ISO 10319:2015; Geosynthetics—Wide-Width Tensile Test. ISO: Geneva, Switzerland, 2015.
31. ISO 9864:2005; Geosynthetics—Test Method for the Determination of Mass per Unit Area of Geotextiles and Geotextile-Related Products. ISO: Geneva, Switzerland, 2005.
32. ASTM D2166-00; Standard Test Method for Unconfined Compressive Strength of Cohesive Soil. ASTM International: West Conshohocken, PA, USA, 2000.
33. Huang, H.; Yuan, Y.; Zhang, W.; Zhu, L. Property Assessment of High-Performance Concrete Containing Three Types of Fibers. *Int. J. Concr. Struct. Mater.* **2021**, *15*, 39. [[CrossRef](#)]

34. Pradhan, S.K.; Pothal, G.K. Shear Strength Characteristics of Pond Ash Reinforced with Polymeric and Natural Fiber Geosynthetic. *Geotech. Geol. Eng.* **2024**, *42*, 3897–3918. [[CrossRef](#)]
35. Wu, Y.; Yamamoto, H.; Cui, J.; Cheng, H. Influence of Load Mode on Particle Crushing Characteristics of Silica Sand at High Stresses. *Int. J. Geomech.* **2020**, *20*, 04019194. [[CrossRef](#)]
36. Fakhrabadi, A.; Ghadakpour, M.; Choobasti, A.J.; Kutanaei, S.S. Influence of the Non-Woven Geotextile (NWG) on the Engineering Properties of Clayey-Sand Treated with Copper Slag-Based Geopolymer. *Constr. Build. Mater.* **2021**, *306*, 124830. [[CrossRef](#)]
37. Que, X.; Zhu, Z.; Zhou, L.; Niu, Z.; Huang, H. Strength and Failure Characteristics of an Irregular Columnar Jointed Rock Mass Under Polyaxial Stress Conditions. *Rock. Mech. Rock. Eng.* **2022**, *55*, 7223–7242. [[CrossRef](#)]
38. Que, X.; Zhu, Z.; He, Y.; Niu, Z.; Huang, H. Strength and Deformation Characteristics of Irregular Columnar Jointed Rock Mass: A Combined Experimental and Theoretical Study. *J. Rock. Mech. Geotech. Eng.* **2023**, *15*, 429–441. [[CrossRef](#)]
39. Wu, Y.; Li, N.; Wang, X.; Cui, J.; Chen, Y.; Wu, Y.; Yamamoto, H. Experimental Investigation on Mechanical Behavior and Particle Crushing of Calcareous Sand Retrieved from South China Sea. *Eng. Geol.* **2021**, *280*, 105932. [[CrossRef](#)]
40. He, H.; Shuang, E.; Lu, D.; Hu, Y.; Yan, C.; Shan, H.; He, C. Deciphering Size-Induced Influence of Carbon Dots on Mechanical Performance of Cement Composites. *Constr. Build. Mater.* **2024**, *425*, 136030. [[CrossRef](#)]
41. Bai, B.; Zhou, R.; Cai, G.; Hu, W.; Yang, G. Coupled Thermo-Hydro-Mechanical Mechanism in View of the Soil Particle Rearrangement of Granular Thermodynamics. *Comput. Geotech.* **2021**, *137*, 104272. [[CrossRef](#)]
42. Bai, B.; Rao, D.; Chang, T.; Guo, Z. A Nonlinear Attachment-Detachment Model with Adsorption Hysteresis for Suspension-Colloidal Transport in Porous Media. *J. Hydrol.* **2019**, *578*, 124080. [[CrossRef](#)]
43. Rowe, R.K.; Hamdan, S. Effect of Wet-Dry Cycles on Standard & Polymer-Amended GCLs in Covers Subjected to Flow over the GCL. *Geotext. Geomembr.* **2021**, *49*, 1165–1175. [[CrossRef](#)]
44. Bai, B.; Nie, Q.; Zhang, Y.; Wang, X.; Hu, W. Cotransport of Heavy Metals and SiO₂ Particles at Different Temperatures by Seepage. *J. Hydrol.* **2021**, *597*, 125771. [[CrossRef](#)]
45. Chen, Y.; Tang, L.; Ye, Y.; Cheng, Z.; Zhou, Z. Effects of Different Chloride Salts on Granite Residual Soil: Properties and Water-Soil Chemical Interaction Mechanisms. *J. Soils Sediments* **2023**, *23*, 1844–1856. [[CrossRef](#)]
46. Chen, Y.; Tang, L.; Sun, Y.; Cheng, Z.; Gong, W. Physical-Mechanical Properties and Microstructure Degradation of Acid-Alkali Contaminated Granite Residual Soil. *Geomech. Energy Environ.* **2023**, *36*, 100501. [[CrossRef](#)]
47. Yuan, B.; Liang, J.; Huang, X.; Huang, Q.; Zhang, B.; Yang, G.; Wang, Y.; Yuan, J.; Wang, H.; Yuan, P. Eco-efficient recycling of engineering muck for manufacturing low-carbon geopolymers via LCA: Exploring the impact of synthesis conditions on performance. *Acta Geotech.* **2024**. [[CrossRef](#)]
48. Yang, B.; Chen, Y.; Zhao, C.; Li, Z. Effect of Geotextiles with Different Masses per Unit Area on Water Loss and Cracking under Bottom Water Loss Soil Conditions. *Geotext. Geomembr.* **2024**, *52*, 233–240. [[CrossRef](#)]
49. Ying, P.; Zhu, Z.; Ren, L.; Deng, S.; Niu, C.; Wan, D.; Wang, F. Deterioration of Dynamic Fracture Characteristics, Tensile Strength and Elastic Modulus of Tight Sandstone under Dry-Wet Cycles. *Theor. Appl. Fract. Mech.* **2020**, *109*, 102698. [[CrossRef](#)]
50. Wu, Y.; Cui, J.; Huang, J.; Zhang, W.; Yoshimoto, N.; Wen, L. Correlation of Critical State Strength Properties with Particle Shape and Surface Fractal Dimension of Clinker Ash. *Int. J. Geomech.* **2021**, *21*, 04021071. [[CrossRef](#)]

Disclaimer/Publisher’s Note: The statements, opinions and data contained in all publications are solely those of the individual author(s) and contributor(s) and not of MDPI and/or the editor(s). MDPI and/or the editor(s) disclaim responsibility for any injury to people or property resulting from any ideas, methods, instructions or products referred to in the content.